Inorganic Chemistry

Article

pubs.acs.org/IC

UiO-68-ol NMOF-Based Fluorescent Sensor for Selective Detection of HClO and Its Application in Bioimaging

Yan-An Li,[§,†] Song Yang,[§,†] Qian-Ying Li,[†] Jian-Ping Ma,[†] Shaojun Zhang,[*,‡] and Yu-Bin Dong[*,†]

[†]College of Chemistry, Chemical Engineering and Materials Science, Collaborative Innovation Center of Functionalized Probes for Chemical Imaging in Universities of Shandong, Key Laboratory of Molecular and Nano Probes, Ministry of Education, Shandong Normal University, Jinan 250014, People's Republic of China

[‡]Shandong Qianfoshan Hospital, Jinan 250014, People's Republic of China

Supporting Information

ABSTRACT: Fluorescent probes are powerful tools for the investigations of reactive oxygen species (ROS) in living organisms by visualization and imaging. As one of the most important of the natural reactive oxygen species (ROS), hypochlorous acid (HClO) plays a crucial role in various physiological and pathological processes. We report herein a new redox-switchable NMOF of **UiO-68-ol** via a direct ligand modification approach. The obtained **UiO-68-ol** NPs, which contains organic-based molecular redox switches, exhibit excellent photophysical properties for biological application and can be highly sensitive and selective fluorescent probes to detect HClO species in living cells.

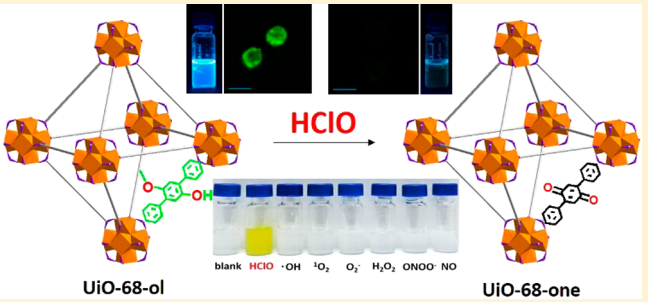

INTRODUCTION

As one of the most important of the natural reactive oxygen species (ROS), hypochlorous acid (HClO) plays a crucial role in various physiological and pathological processes. Endogenous HClO in living cells, such as neutrophils, macrophages, and monocytes, is known to be generated by myeloperoxidase (MPO)-catalyzed peroxidation of chloride ions.[1] Although it might be able to injure some invasive microorganisms during biomolecular chemical modification processes, excessive HClO can also result in a variety of human diseases such as inflammatory diseases, cardiovascular diseases, cancer, and neurodegeneration.[2] Therefore, monitoring the level of intracellular HClO species is of great interest and significance for elucidating the role of HClO in various biological processes.

As a promising method, fluorescence imaging technology is widely used in monitoring HClO species in living cells due to its high spatial and temporal resolution.[3] So far, small organic fluorescent molecules might be the most widely used probes to detect HClO in living systems.[4] These reported fluorescent probes contain HClO recognition functional groups which can respond to HClO and, furthermore, differentiate it from other kinds of ROS species. However, some known HClO fluorescent probes do not have good performance in real-time monitoring of the HClO level in living systems due to their delayed response time.[5] Therefore, the development of new types of fluorescent bioprobes in living cells is imperative. We have initiated a synthetic program for the preparation of bioprobes based on nanoscale metal−organic frameworks (NMOFs),[6] in which the concepts of organic-based molecular sensors (OMSs) and NMOFs were combined to yield NMOF probes that are able to quickly detect some target analytes in living cells with high selectivity and sensitivity.[7]

In this contribution, a new redox-switchable UiO-type of NMOF, **UiO-68-ol**, which was generated from the functionalized bicarboxylic acid ligand $\mathbf{H_2L}$**-ol** and Zr(IV) salt (Scheme 1), is reported. It can be a highly sensitive and specific fluorescence probe to detect HClO in living cells. The design and synthesis of **UiO-68-ol** are based on the following reasons. First, UiO-type MOFs are known to be very stable in aqueous media, and they possess large internal pores which can facilitate the accommodation of the OMS and the contact between the OMS and the target analyte.[8] Second, UiO-type NMOFs have low toxicity[9] and possess good cellular biocompatibility and membrane permeability, which allows them to be suitable for bioimaging.[9] Third, the incorporation of OMSs into periodic and porous NMOFs via covalent bonding interactions would effectively prevent not only aggregation-caused quenching (ACQ)[10] but also dye leaching. Hopefully, these types of NMOF-based probes can exhibit higher sensing and bioimaging performance in comparison to the corresponding small organic molecular sensors.

EXPERIMENTAL SECTION

Materials and Instrumentation. All of the starting materials were purchased from commercial sources, unless otherwise noted, and used without further purification. Infrared (IR) samples were prepared as KBr pellets, and spectra were obtained in the 400−4000 cm^{-1} range

Received: August 5, 2017

DOI: 10.1021/acs.inorgchem.7b02012
Inorg. Chem. XXXX, XXX, XXX−XXX

Scheme 1. Synthesis of H_2L-ol (Top) and UiO-68-ol (Bottom)[a]

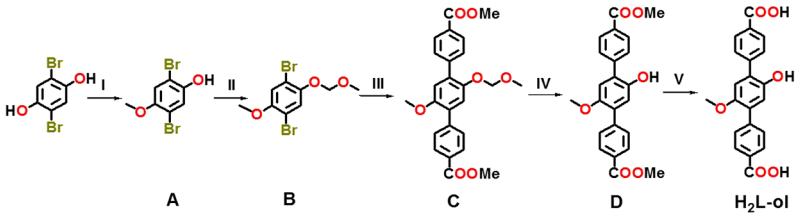

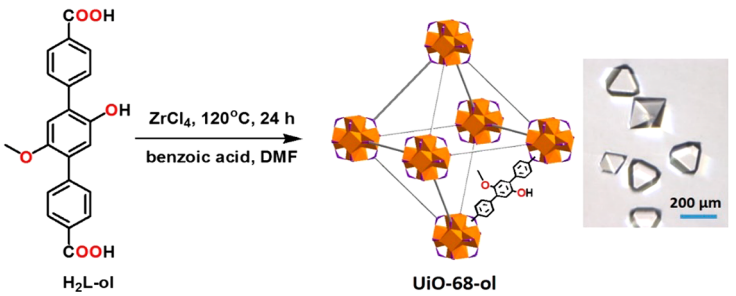

[a]A photograph of the **UiO-68-ol** single crystals is given as an insert.

using a PerkinElmer 1600 FTIR spectrometer. ^{1}H NMR data were collected using an AM-400 spectrometer. Chemical shifts are reported in δ relative to TMS. Fluorescence spectra were obtained with an FLS-920 Edinburgh Fluorescence Spectrometer with a xenon lamp. The scanning electron microscopy (SEM) micrographs were recorded on a Gemini Zeiss Supra TM scanning electron microscope. The X-ray diffraction (XRD) experiments were obtained on a D8 ADVANCE X-ray powder diffractometer with Cu Kα radiation (λ = 1.5405 Å). The Brunauer−Emmett−Teller (BET) surface area was measured on an ASAP 2020/TriStar 3000instrument (Micromeritics) using nitrogen adsorption at 77 K. Confocal fluorescence imaging studies were performed with a TCS SP5 confocal laser scanning microscope (Leica Co., Ltd. Germany) with an objective lens (×20). The microscope images of crystals were collected on a Leica DMI3000B inverted microscope. The UV−vis absorption spectra were recorded on a Shimadzu UV-3600 spectrophotometer. The crystal data were obtained with an Agilent SuperNova X-ray single-crystal diffractometer.

^{1}H NMR Measurement on the Digested MOFs. In a typical procedure, the activated MOF sample (ca. 10 mg) was digested with sonication in 1 mL of DMSO and 10 μL of 30% HF aqueous solution. Upon addition of water (ca. 5 mL), the precipitate was washed and collected for ^{1}H NMR study.

Synthesis of UiO-68-ol Bulk Crystals and Their Redox Reactions. $ZrCl_4$ (11.2 mg, 0.048 mmol), **H_2L-ol** (25 mg, 0.07 mmol), and C_6H_5COOH (222.6 mg, 1.82 mmol) were dissolved in DMF (3 mL). The tightly capped flasks were kept in an oven at 120 °C under static conditions. After 24 h, the reaction system was cooled to room temperature and the bulk colorless crystals were obtained in 43% yield. The crystals were suspended in fresh DMF (10 mL) overnight. After they were soaked in methylene chloride for 3 days, the crystals were centrifuged and dried. IR (KBr pellet, cm^{-1}): 3412 (m), 1722 (s), 1614 (s), 1477 (m), 1305 (s), 1286 (s), 1217 (m), 1192 (s), 1055 (m), 801 (s), 709 (s), 517 (w). ^{1}H NMR (400 MHz, DMSO-d_6, 25 °C, TMS, ppm): 12.97 (s, 2H, −COOH), 9.50 (s, 1H, −OH), 8.02−7.98 (d, 2H, $-C_6H_4-$), 7.96−7.93 (d, 2H, $-C_6H_4-$), 7.81−7.79 (d, 2H, $-C_6H_4-$), 7.63−7.61 (d, 2H, $-C_6H_4-$), 7.08 (s, 1H, $-C_6H_2-$), 6.96 (s, 1H, $-C_6H_2-$), 3.77 (s, 3H, $-CH_3$).

When **UiO-68-ol** (10 mg) was immersed in a phosphate buffered saline (PBS) solution of NaClO (10^{-3} M, 10 mL, pH 7.4) for 15 min, the colorless crystals turned yellow to generate **UiO-68-one** in 95% yield. IR (KBr pellet, cm^{-1}): 3001 (m), 1702 (s), 1644 (s), 1402 (m), 1286 (s), 1199 (m), 1128 (s), 861 (s), 774 (s), 542 (w). ^{1}H NMR (400 MHz, DMSO-d_6, 25 °C, TMS, ppm): 13.17 (s, 2H, −COOH), 8.04−8.02 (d, 4H, $-C_6H_4-$), 7.72−7.70 (d, 4H, $-C_6H_4-$), 7.18 (s, 2H, $-C_6H_2-$).

The obtained **UiO-68-one** (10 mg) was further immersed in a PBS solution of ascorbic acid (VC; 2.5 mg/mL) for 15 min, and the yellow crystals turned colorless to generate **UiO-68-ol′** quantitatively. IR (KBr pellet, cm^{-1}): 3455 (m), 2671 (w), 1674 (s), 1617(s), 1419 (s), 1395 (s), 1286 (s), 1211 (w), 1180 (m), 1009 (w), 851 (w), 765 (m), 562 (w). ^{1}H NMR (400 MHz, DMSO-d_6, 25 °C, TMS, ppm): 12.95 (s, 2H, −COOH), 9.26 (s, 2H, −OH), 8.00−7.98 (d, 4H, $-C_6H_4-$), 7.71−7.69 (d, 4H, $-C_6H_4-$), 6.93 (s, 2H, $-C_6H_2-$).

Synthesis of UiO-68-ol Nanocrystals and Their Redox Reactions. $ZrCl_4$ (9.6 mg, 0.040 mmol), **H_2L-ol** (14.56 mg, 0.040 mmol), and CH_3COOH (240 μL) were dissolved in DMF (3.2 mL). The tightly capped flasks were kept in an oven at 120 °C under static conditions. After 24 h, the reaction system was cooled to room temperature and nanocrystals were obtained (41% yield). The nanocrystals were suspended in fresh DMF (10 mL) overnight. After they were soaked in methylene chloride for 3 days, the nanocrystals were centrifuged and dried at 80 °C. IR (KBr pellet, cm^{-1}): 3412 (m), 1722 (s), 1614 (s), 1477 (m), 1305 (s), 1286 (s), 1217 (m), 1192 (s), 1055 (m), 801 (s), 709 (s), 517 (w). ^{1}H NMR (400 MHz, DMSO-d_6, 25 °C, TMS, ppm): 12.97 (s, 2H, −COOH), 9.50 (s, 1H, −OH), 8.02−7.98 (d, 2H, $-C_6H_4-$), 7.96−7.93 (d, 2H, $-C_6H_4-$), 7.81−7.79 (d, 2H, $-C_6H_4-$), 7.63−7.61 (d, 2H, $-C_6H_4-$), 7.08 (s, 1H, $-C_6H_2-$), 6.96 (s, 1H, $-C_6H_2-$), 3.77 (s, 3H, $-CH_3$).

When a PBS solution (900 μL) of **UiO-68-ol** (1 mg) was combined with a PBS solution of NaClO (10^{-3} M, 100 μL), the mixture changed from colorless to yellow immediately. The obtained yellow solution promptly changed back to colorless once a PBS solution of VC (10^{-3} M, 150 μL) was added. This redox process was further demonstrated by the emission spectra.

Cell Culture and Treatments. The RAW264.7 cell lines were provided by the Institute of Basic Medicine, Shandong Academy of Medical Sciences (People's Republic of China). The cells were grown in DMEM (Invitrogen, CA, USA) containing 10% heat-inactivated newborn calf serum, 100 U/mL penicillin, and 100 mg/mL streptomycin under an atmosphere of 5% CO_2 and 95% air at 37 °C. For confocal fluorescence imaging, cells were incubated in glass-bottom dishes for 24 h. Cells were incubated at 37 °C with 10 mg/L **UiO-68-ol** in PBS (phosphate buffered saline) for 1 h and washed with PBS, and fluorescence images were captured. In a control experiment, RAW264.7 cells were pretreated with PMA (phorbol-12-myristate-13-acetate; 1.5 mg/L) for different times under an atmosphere of 5% CO_2 and 95% air at 37 °C and then washed with PBS. These cells were

DOI: 10.1021/acs.inorgchem.7b02012
Inorg. Chem. XXXX, XXX, XXX−XXX

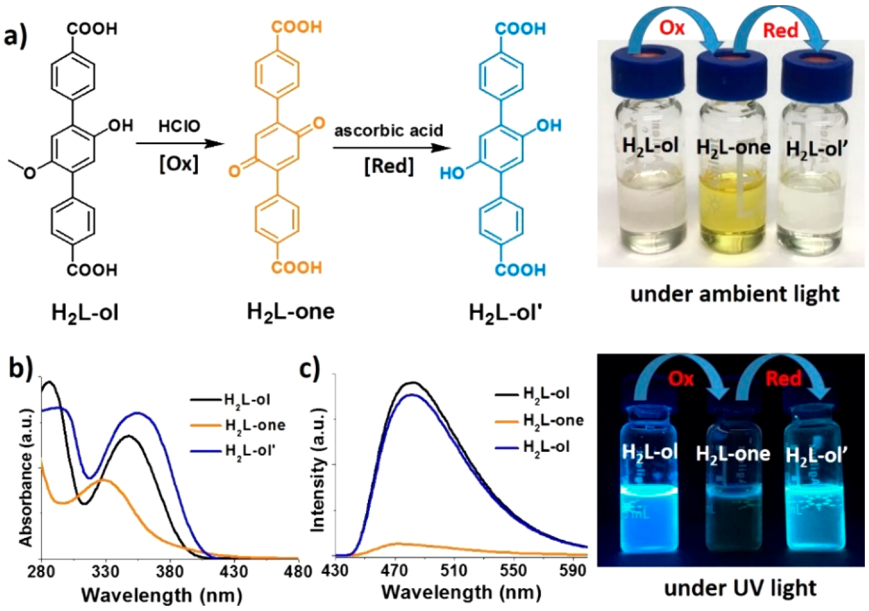

Figure 1. (a) Redox reactions based on **H_2L-ol**. Photographs of **H_2L-ol**, **H_2L-one**, and **H_2L-ol′** in PBS under ambient light are given as an insert. (b) UV−vis spectra of **H_2L-ol**, **H_2L-one**, and **H_2L-ol′**. (c) Fluorescence spectra of **H_2L-ol**, **H_2L-one**, and **H_2L-ol′** (λ_{ex} 405 nm, λ_{em} 482 nm). Photographs of **H_2L-ol**, **H_2L-one**, and **H_2L-ol′** in PBS under UV light are given as an insert.

further loaded with 10 mg/L **UiO-68-ol** for 1 h and washed with PBS. In another control experiment, RAW264.7 cells were pretreated with PMA (1.5 mg/mL) for 30 min under an atmosphere of 5% CO_2 and 95% air at 37 °C and then washed with PBS; these cells were loaded with 10 mg/L **UiO-68-ol** for 1 h and washed with PBS. These cells were further loaded with 2 mg/L VC for different times and washed with PBS. Samples were excited at 405 nm and observed between 500 and 550 nm.

X-ray Structural Determination.[11] X-ray intensity data were measured at 100 K on an Agilent SuperNova CCD-based diffractometer (Cu Kα radiation, λ = 1.54184 Å). After a determination of crystal quality and initial tetragonal unit cell parameters, a hemisphere of frame data was collected. The raw data frames were integrated with CrysAlisPro (compiled Aug 2, 2013, 16:46:58). Empirical absorption correction used spherical harmonics, implemented in the SCALE3 ABSPACK scaling algorithm. Analysis of the data showed negligible crystal decay during data collection. The structure was solved by a combination of direct methods and difference Fourier syntheses and refined by full-matrix least squares against F^2, using the SHELXTL software package. A large void space is present in the framework, which contains many significant electron density peaks. The species in this region were too severely disordered to be modeled and were treated with SQUEEZE/PLATON. The functional groups at the central benzene ring are statistically disordered and subject to large thermal vibration and disorder. They were not resolved in the electron map and have been omitted from the structural model. The sum formula given is for the actual compound including the substituents at the central benzene ring, but unresolved solvate molecules were ignored. A crystal data and structure determination summary for **UiO-68-ol** are given in Table S1 in the Supporting Information. CCDC 1564073 contains the supplementary crystallographic data for this paper. These data can be obtained free of charge from The Cambridge Crystallographic Data Centre via www.ccdc.cam.ac.uk/data_request/cif.

RESULTS AND DISCUSSION

Synthesis and Characterization of H_2L-ol and Its Redox Property. As shown in Scheme 1, the *p*-methyloxyphenol-containing redox-switchable ligand **H_2L-ol** was prepared through a multistep synthetic processure (Supporting Information). For examination of its redox-switchable behavior, **H_2L-ol** was conbined with HClO (0.1 M, 1 mL of NaClO; 12 M, 5 μL of HCl) in phosphate buffer (PBS, 0.2 M) for 20 min; **H_2L-one** was generated in ca. 95% yield on the basis of ^{1}H NMR measurements (Figure 1a and the Supporting Information). After further treament of the obtained **H_2L-one** by ascorbic acid (VC) in DMSO at room temerpature for 15 min, the reduced product of **H_2L-ol′** was quantitatively obtained on the basis of a ^{1}H NMR spectrum (Figure 1a and the Supporting Information). In the ^{1}H NMR spectra, the single peak for −OH at 9.49 ppm (1H) of **H_2L-ol** disappeared after the HClO treament, and it reappeared at 9.26 ppm (2H) after the addition of VC (Supporting Information). In comparison to **H_2L-ol** and **H_2L-ol′**, the IR spectrum of **H_2L-one** showed a 1650 cm^{-1} adsorption derived from the >C═O group, which is reflected in the oxidation restricted to the −OH and $-OCH_3$ moieties on the central benzene ring (Supporting Information).

Interestingly, this redox process was accompanied by a visual colorless to yellow to colorless color change (Figure 1a), which is auite consistent with the UV−vis spectra (Figure 1b). More importantly, the fluorescence intensity also went through a dramatic change during this redox process. As shown in Figure 1c, the strong fluorescence of **H_2L-ol** (λ_{ex} 405 nm, λ_{em} 482 nm) was almost quenched after treatment with HClO. On the other hand, the blue emission was largely recovered (ca. 92%) after the reduction of **H_2L-one** to **H_2L-ol′** by VC (Figure 1c).

Synthesis and Characterization of UiO-68-ol and Its Redox Properties. With this redox-switchable ligand **H_2L-ol** in hand, we designed and prepared the Zr(IV)-MOF based on it. The combination of **H_2L-ol** and $ZrCl_4$ under solvothermal conditions (DMF, C_6H_5COOH, 120 °C, 24 h) afforded bulk **UiO-68-ol** colorless crystals in 43% yield (Scheme 1). In addition to the ^{1}H NMR spectrum and thermogravimetric analysis (TGA, Supporting Information), single-crystal X-ray diffraction was also used to characterize **UiO-68-ol**, and this revealed that **UiO-68-ol** ($C_{63}H_{48}O_{30}Zr_3$) crystallized in the cubic space group $Fm\bar{3}m$. It is isostructural with the pristine **UiO-68**.

DOI: 10.1021/acs.inorgchem.7b02012
Inorg. Chem. XXXX, XXX, XXX−XXX

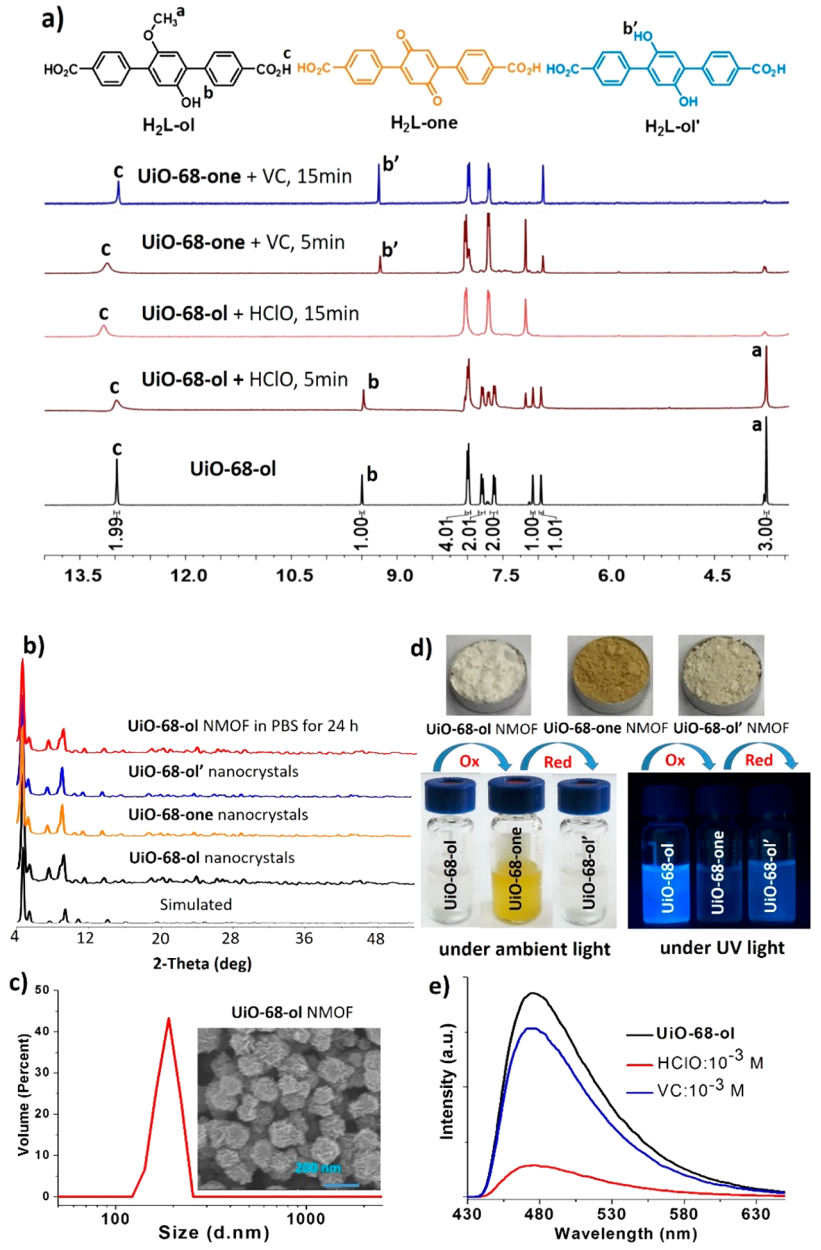

Figure 2. (a) *p*-Methyloxyphenol/quinone/hydroquinone redox reactions on the bulk crystals monitored by the ^{1}H NMR (DMSO-d_6) spectra performed on the digested crystals. (b) PXRD patterns of **UiO-68-ol**, **UiO-68-one**, **UiO-68-ol'**, and **UiO-68-ol** NMOFs in PBS for 24 h. (c) Dynamic light scattering (DLS) measurement of **UiO-68-ol** and its SEM image. (d) Photographs of PBS solutions of **UiO-68-ol**, **UiO-68-one**, and **UiO-68-ol'** NMOFs under ambient light and on excitation with a mercury lamp. Photographs of **UiO-68-ol**, **UiO-68-one**, and **UiO-68-ol'** samples are given as an insert. (e) Fluorescence change of **UiO-68-ol** PBS solution upon successive addition of HClO and VC (λ_{ex} 405 nm, λ_{em} 475 nm).

Due to the redox-switchable **H$_2$L-ol** involved, we anticipated that the generated **UiO-68-ol** bulk crystals could also feature a similar fluorescence switching behavior in the solid state. As expected, **UiO-68-ol** is indeed a redox-switchable MOF, and its redox-switching process was monitored on the digested bulk crystals by the ^{1}H NMR spectra. As indicated in Figure 2a, the ^{1}H NMR spectra showed that the −OH proton at δ 9.50 ppm in **UiO-68-ol** gradually disappeared (ca. 15 min) upon addition of NaClO (10^{-3} M, 100 μL), indicating that **UiO-68-one** had formed (ca. 95% yield). After treament of the generated **UiO-68-one** by VC (10^{-3} M, 150 μL) for 15 min, the −OH proton peak appeared again (δ 9.30 ppm), but the integral area corresponded to two −OH protons. Meanwhile, basically no proton resonance for $-OCH_3$ was found in the upfield region (δ 3.80 ppm) with respect to the loss of the methyl group, indicating the generation of the reduced product of **UiO-68-ol'** in nearly quantitative yield. This observation confirmed that **UiO-68-ol** bulk crystals indeed exhibited redox-switching properties and the chemical transformation occurred on the central *p*-methyloxyphenol and *p*-benzoquinone rings through the *p*-methyloxyphenol/quinone/hydroquinone redox reactions,[12] which are the same as those of **H$_2$L-ol**.

For detecting HClO species in living cells, **UiO-68-ol** NMOFs were prepared by using acetic acid instead of benzoic acid to perform the solvothermal synthetic reaction (DMF, CH_3COOH, 120 °C, 24 h). As shown in Figure 2b, the obtained **UiO-68-ol** NMOFs feature the same structural pattern as that of bulk single crystals on the basis of the

DOI: 10.1021/acs.inorgchem.7b02012
Inorg. Chem. XXXX, XXX, XXX−XXX

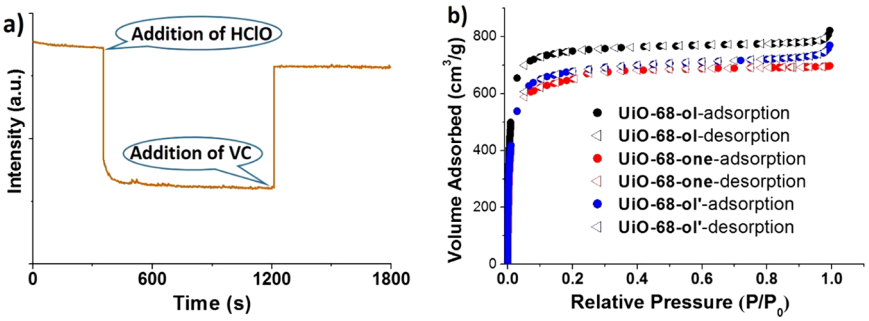

Figure 3. (a) Time-dependent fluorescence spectra of **UiO-68-ol** with sequential addition of HClO and VC. (b) N_2 adsorption isotherms for **UiO-68-ol**, **UiO-68-one**, and **UiO-68-ol′** at 77 K.

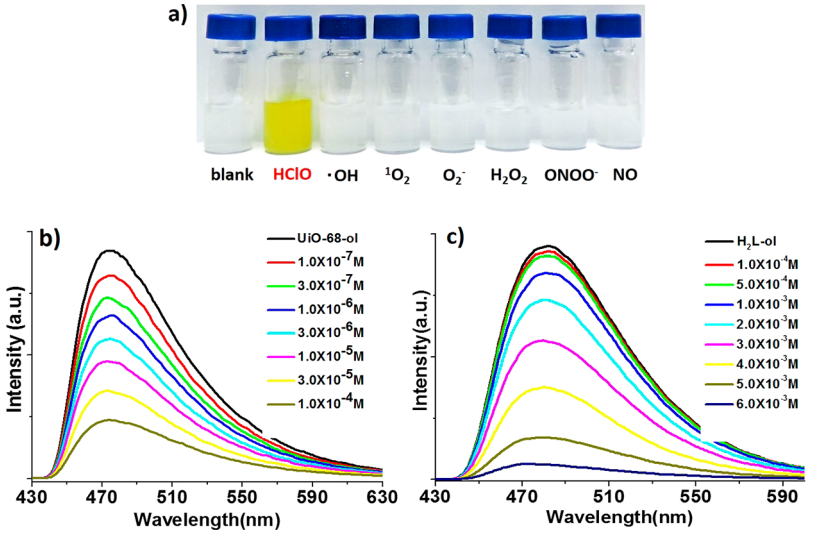

Figure 4. (a) Color change of **UiO-68-ol** (1 mg, 0.2 M PBS, 900 μL) in the presence of various representative ROSs, from left to right: blank, HClO, $^{\bullet}$OH, $^1O_2$, O_2^-, H_2O_2, $ONOO^-$, and NO. [ROS] = 10^{-3} M. (b) Luminescence spectra of **UiO-68-ol** (0.1 mg/mL) upon addition of HClO at different concentrations in PBS, respectively. The emission maximum was observed at 475 nm (λ_{ex} 405 nm). K_{sv} = 1.21 × 10^6 L mol^{-1}. (c) Luminescence spectra of **H_2L-ol** (0.073 mg/mL) upon addition of HClO at different concentrations in PBS, respectively. The emission maximum was observed at ca. 482 nm (λ_{ex} 405 nm). K_{sv} = 1.30 × 10^2 L mol^{-1}. Each individual spectrum was recorded after incubation of the probes with the HClO analyte within 5 s.

PXRD patterns. A scanning electron microscopy (SEM) image demonstrated that the generated **UiO-68-ol** NMOF particles were uniformly distributed (Figure 2c), and their size is centered at ca. 170 nm, which is well supported by a dynamic light scattering (DLS) measurement (Figure 2c). As shown in Figure 2d, when a solution of **UiO-68-ol** NPs (1 mg) in PBS (900 μL, 0.2 M) was added to a PBS solution of NaClO (10^{-3} M), the system turned from colorless to yellow immediately. Considering that the pK_a of HClO is 7.46, we concluded that **UiO-68-ol** herein responded to HClO rather than ClO^-, similar to the behavior of other organic molecular fluorescence probes reported previously.[4a,b] After addition of VC (10^{-3} M), the system promptly turned back to colorless. The redox transformation on **UiO-68-ol** NPs is also accompanied by a drastic fluorescence change. As indicated in Figure 2d,e, **UiO-68-ol** NPs in PBS solution showed a bright blue emission at 475 nm, whereas **UiO-68-one** NPs were basically non-fluorescent. After further reduction of **UiO-68-one**, the **UiO-68-ol′** NPs had a blue emission again (recovered by 82%). Therefore, **UiO-68-ol** NMOF exhibited the same redox-switchable phenomenon as those of **H_2L-ol** and **UiO-68-ol** bulk crystals and the structural integrity of **UiO-68-ol** was well preserved during the redox process, which is well demonstrated by the PXRD patterns (Figure 2b) and their TEM images (Supporting Information). In addition, the PXRD pattern further confirms that the **UiO-68-ol** NMOF is very stable in PBS solution (Figure 2b). Such an NMOF would be a good candidate as a fluorescence probe for bioimaging in living cells.

To our delight, the redox-switching processes on the **UiO-68-ol** and **UiO-68-one** NPs are very fast, and the whole redox response time is within only ca. 3 s (Figure 3a). We believe this quick response can be ascribed to the large surface areas of the NMOFs. As shown in Figure 3b, all three NMOFs exhibited microporous material features. The Brunauer−Emmett−Teller (BET) surface areas were found to be 2517.3, 2198.8, and 2302.6 m^2/g, respectively, indicating their high porosity. Logically, the nanosize of the NMOFs, together with their porous nature, should dramatically increase the probe/analyte contacting probability and consequently the quick respone.

In addition, the selectivity of **UiO-68-ol** for other kinds of ROSs was also investigated. We were pleased to find that **UiO-68-ol** was stable toward most other common ROS species, such as $^{\bullet}$OH, $^1O_2$, H_2O_2, $ONOO^-$, and NO, as presented in Figure 4a. Thus, the oxidation of **UiO-68-ol** to **UiO-68-one** is specific for HClO. As mentioned above, it is a ligand-based redox process, and only HClO instead of other ROS species can be an

DOI: 10.1021/acs.inorgchem.7b02012
Inorg. Chem. XXXX, XXX, XXX−XXX

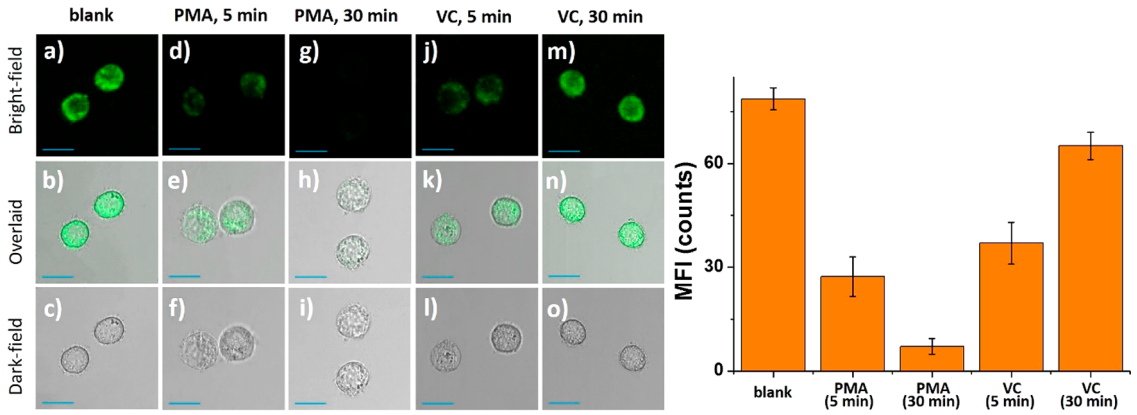

Figure 5. (left) Overlaid DIC confocal fluorescence images of living RAW264.7 cells. The cells were incubated with 10 mg/L **UiO-68-ol** in PBS for 1 h (a–c). RAW264.7 cells were pretreated with PMA (1.5 mg/L) for 5 (d–f) and 30 min (g–i) and further incubated with 10 mg/L **UiO-68-ol** for 1 h. RAW264.7 cells (g–j) were incubated with 2 mg/L VC for 5 (j–l) and 30 min (m–o). Incubation was performed at 37 °C under a humidified atmosphere containing 5% CO_2. The emission wavelengths are 500–550 nm (λ_{ex} 405 nm). Scale bars are 25 μm. (right) The corresponding mean fluorescence intensity (MFI) of RAW264.7 cells. The observation indicates that the emission of **UiO-68-ol** in living cells was quenched by HClO and further recovered after treatment with VC.

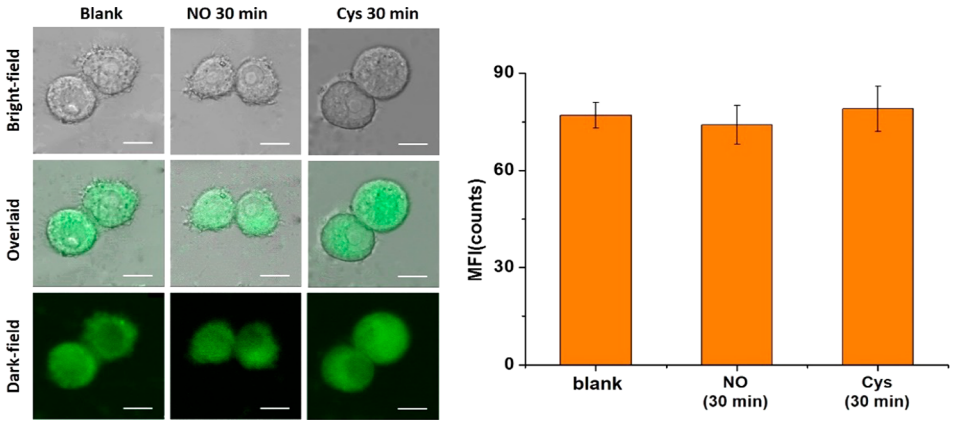

Figure 6. RAW264.7 cells pretreated with NONOate (1,1-diethyl-2-hydroxy-2-nitrosohydrazine; 30 μM)/Cys (30 μM) for 30 min under an atmosphere of 5% CO_2 and 95% air at 37 °C and then washed with PBS. These cells were further loaded with 10 mg/L **UiO-68-ol** for 1 h and washed with PBS. Samples were excited at 405 nm and observed between 500 and 550 nm. Scale bars are 10 μm.

effective oxidant to trigger the −OH to >C═O transformation on the ligand, which resulted in the high selectivity of **UiO-68-ol** NMOF for HClO (Supporting Information). We next evaluated the detection limit of **UiO-68-ol** for HClO under simulated physiological conditions on the basis of luminescence spectra. The corresponding emission spectra toward HClO based on **UiO-68-ol** are shown in Figure 4b. The reactions of the **UiO-68-ol** NMOF with HClO at different concentrations were carried out, and good linearity between the relative fluorescent intensities and the concentrations of the HClO species in the range of 10^{-7}–10^{-4} M was observed (linear coefficient 0.9930, Supporting Information), indicating that the detection limit for HClO on the basis of the proposed method is ca. 10^{-7} M. In contrast, the HClO detection limit on the basis of **H_2L-ol** is only ca. 10^{-3} M (with a linear coefficient of 0.9914 within (1–6) × 10^{-3} M, Figure 4c and the Supporting Information). The much higher sensitivity exhibited by the NMOFs rationally resulted from the ordered arrangement of the HClO-reactive groups in the rigid frameworks in the solid state, which could effectively prevent their aggregate formation and consequently the ACQ effect. Additionally, the redox reactions directly occurred on the host framework rather than the encapsulated dye guest; thus, the dye leaching problem can be completely avoided. Interestingly, the **UiO-68-ol** NMOF can be reused, but according to the **UiO-68-ol → UiO-68-one → UiO-68-ol′ → UiO-68-one → UiO-68-ol′ → UiO-68-one** cycle (Supporting Information).

Bioimaging of HClO in Living Cells Based on UiO-68-ol. By taking advantage of the high selectivity and sensitivity, we finally employed **UiO-68-ol** NMOFs to image HClO in living cells. When RAW264.7 cells were incubated with **UiO-68-ol** NPs for 1 h, a bright fluorescence in the green channel was clearly observed, indicating that **UiO-68-ol** NPs have good membrane permeability. Notably, the emission intensity of **UiO-68-ol** significantly decreased upon stimulation with phorbol-12-myristate-13-acetate (PMA, 1.5 mg/L). As shown in Figure 5, the bright green emission gradually dimmed as time went on, and the emission was almost completely quenched at 30 min, indicating that **UiO-68-ol** is able to respond to intracellular HClO and, furthermore, can detect the change in HClO at different levels under ambient conditions. On the other hand, the luminescence in the green channel can also be largely recovered by reduction back to hydroquinone (Figure 5). This redox-based fluorescence "turn-off-on" process was further demonstrated by the mean fluorescence intensity (MFI). As shown in Figure 5, the mean fluorescence intensity

DOI: 10.1021/acs.inorgchem.7b02012
Inorg. Chem. XXXX, XXX, XXX–XXX

(MFI) in RAW264.7 cells decreased by 50 and 91% after treament with PMA for 5 and 30 min, respectively. Furthermore, the fluorescence intensity in RAW264.7 cells was effectively recovered after addition of VC, and it increased by 50 and 83% at 5 and 30 min, respectively. Such observation is consistent with that of the redox-switching phenomenon exhibited by **H_2L-ol** ligand and **UiO-68-ol** bulk crystals.

To further confirm the selectivity of **UiO-68-ol** for HClO species in living cells, the fluorescence response of **UiO-68-ol** to RNS and RSS, which are two types of important bioactive species in living cells, was also examined. NO and cysteine (Cys) were chosen to perform the bioimaging experiments. As shown in Figure 6, NO and Cys could not cause an intensity decrease of green fluorescence with excitation at 405 nm, which is drastically distinct from the case for HClO. Therefore, NO and Cys cannot disturb the HClO detection and the **UiO-68-ol** MOF probe shows very high specificity to the detection of HClO in living cells.

CONCLUSION

In summary, we prepared the new redox-switchable NMOF **UiO-68-ol** via a direct ligand modification approach, in which the organic-based molecular switches are grafted on MOFs. It exhibits excellent photophysical properties for biological applications and can be a highly sensitive and selective fluorescent probe to detect HClO species in living cells. We expect this approach to be viable for the construction of many more new and interesting fluorescent MOF probes of this type, and studies toward the preparation of new MOF-based fluorescent sensoring systems for detecting other kinds of analytes are underway.

ASSOCIATED CONTENT

Supporting Information

The Supporting Information is available free of charge on the ACS Publications website at DOI: 10.1021/acs.inorgchem.7b02012.

Ligand synthesis, additional characterization data for the redox reactions, detection limit measurements, and an ORTEP figure and single-crystal data for CCDC 1564073 (PDF)

Accession Codes

CCDC 1564073 contains the supplementary crystallographic data for this paper. These data can be obtained free of charge via www.ccdc.cam.ac.uk/data_request/cif, or by emailing data_request@ccdc.cam.ac.uk, or by contacting The Cambridge Crystallographic Data Centre, 12 Union Road, Cambridge CB2 1EZ, UK; fax: +44 1223 336033.

AUTHOR INFORMATION

Corresponding Authors

*E-mail for S.Z.: vickie5454@163.com.
*E-mail for Y.-B.D.: yubindong@sdnu.edu.cn.

ORCID

Yu-Bin Dong: 0000-0002-9698-8863

Author Contributions

§Y.-A.L. and S.Y. contributed equally.

Notes

The authors declare no competing financial interest.

ACKNOWLEDGMENTS

We are grateful for financial support from the NSFC (Grant Nos. 21671122 and 21475078) and the Taishan Scholar's Construction Project.

REFERENCES

(1) (a) Harrison, J. E.; Schultz, J. Studies on the Chlorinating Activity of Myeloperoxidase. *J. Biol. Chem.* **1976**, *251*, 1371−1374. (b) Winterbourn, C. C. Myeloperoxidase as an Effective Inhibitor of Hydroxyl Radical Production. Implications for the Oxidative Reactions of Neutrophils. *J. Clin. Invest.* **1986**, *78*, 545−550.

(2) (a) Sugiyama, S.; Okada, Y.; Sukhova, G. K.; Virmani, R.; Heinecke, J. W.; Libby, P. Macrophage Myeloperoxidase Regulation by Granulocyte Macrophage Colony-Stimulating Factor in Human Atherosclerosis and Implications in Acute Coronary Syndromes. *Am. J. Pathol.* **2001**, *158*, 879−891. (b) Wu, S. M.; Pizzo, S. V. α2-Macroglobulin from Rheumatoid Arthritis Synovial Fluid: Functional Analysis Defines a Role for Oxidation in Inflammation. *Arch. Biochem. Biophys.* **2001**, *391*, 119−126. (c) Hammerschmidt, S.; Büchler, N.; Wahn, H. Tissue Lipid Peroxidation and Reduced Glutathione Depletion in Hypochlorite-induced Lung Injury*. *Chest* **2002**, *121*, 573−581. (d) Hasegawa, T.; Malle, E.; Farhood, A.; Jaeschke, H. Generation of Hypochlorite-modified Proteins by Neutrophils during Ischemia-reperfusion Injury in Rat Liver: Attenuation by Ischemic Preconditioning. *Am. J. Physiol. Gastrointest. Liver. Physiol.* **2005**, *289*, G760−G767.

(3) Chen, X.; Tian, X.; Shin, I.; Yoon, J. Fluorescent and Luminescent Probes for Detection of Reactive Oxygen and Nitrogen Species. *Chem. Soc. Rev.* **2011**, *40*, 4783−4804.

(4) (a) Shepherd, J.; Hilderbrand, S. A.; Waterman, P.; Heinecke, J. W.; Weissleder, R.; Libby, P. A Fluorescent Probe for the Detection of Myeloperoxidase Activity in Atherosclerosis-Associated Macrophages. *Chem. Biol.* **2007**, *14*, 1221−1223. (b) Kenmoku, S.; Urano, Y.; Kojima, H.; Nagano, T. Development of a Highly Specific Rhodamine-Based Fluorescence Probe for Hypochlorous Acid and Its Application to Real-Time Imaging of Phagocytosis. *J. Am. Chem. Soc.* **2007**, *129*, 7313−7316. (c) Sun, Z. N.; Liu, F. Q.; Chen, Y.; Tam, P. K. H.; Yang, D. A Highly Specific BODIPY-Based Fluorescent Probe for the Detection of Hypochlorous Acid. *Org. Lett.* **2008**, *10*, 2171−2174. (d) Chen, X.; Wang, X.; Wang, S.; Shi, W.; Wang, K.; Ma, H. A Highly Selective and Sensitive Fluorescence Probe for the Hypochlorite Anion. *Chem. - Eur. J.* **2008**, *14*, 4719−4724. (e) Yang, Y.-K.; Cho, H. J.; Lee, J.; Shin, I.; Tae, J. A Rhodamine−Hydroxamic Acid-Based Fluorescent Probe for Hypochlorous Acid and Its Applications to Biological Imagings. *Org. Lett.* **2009**, *11*, 859−861. (f) Lou, Z.; Li, P.; Pan, Q.; Han, K. A Reversible Fluorescent Probe for Detecting Hypochloric Acid in Living Cells and Animals: Utilizing a Novel Strategy for Effectively Modulating the Fluorescence of Selenide and Selenoxide. *Chem. Commun.* **2013**, *49*, 2445−2447. (g) Zhu, H.; Fan, J.; Wang, J.; Mu, H.; Peng, X. An "Enhanced PET"-Based Fluorescent Probe with Ultrasensitivity for Imaging Basal and Elesclomol-Induced HClO in Cancer Cells. *J. Am. Chem. Soc.* **2014**, *136*, 12820−12823. (h) Zhang, R.; Zhao, J.; Han, G.; Liu, Z.; Liu, C.; Zhang, C.; Liu, R.; Jiang, C.; Liu, R.; Zhao, T.; Han, M.-Y.; Zhang, Z. Real-Time Discrimination and Versatile Profiling of Spontaneous Reactive Oxygen Species in Living Organisms with a Single Fluorescent Probe. *J. Am. Chem. Soc.* **2016**, *138*, 3769−3778.

(5) (a) Liu, F.; Wu, T.; Cao, J.; Zhang, H.; Hu, M.; Sun, S.; Song, F.; Fan, J.; Wang, J.; Peng, X. A Novel Fluorescent Sensor for Detection of Highly Reactive Oxygen Species, and for Imaging Such Endogenous ROS in the Mitochondria of Living Cells. *Analyst* **2013**, *138*, 775−778. (b) Lou, Z.; Li, P.; Song, P.; Han, K. Ratiometric Fluorescence Imaging of Cellular Hypochlorous Acid based on Heptamethine Cyanine Dyes. *Analyst* **2013**, *138*, 6291−6295.

(6) (a) Della Rocca, J.; Liu, D.; Lin, W. Nanoscale Metal−Organic Frameworks for Biomedical Imaging and Drug Delivery. *Acc. Chem. Res.* **2011**, *44*, 957−968. (b) He, C.; Liu, D.; Lin, W. Nanomedicine Applications of Hybrid Nanomaterials Built from Metal−Ligand

DOI: 10.1021/acs.inorgchem.7b02012
Inorg. Chem. XXXX, XXX, XXX−XXX

Coordination Bonds: Nanoscale Metal−Organic Frameworks and Nanoscale Coordination Polymers. *Chem. Rev.* **2015**, *115*, 11079−11108. (c) Li, B.; Wen, H.-M.; Cui, Y.; Zhou, W.; Qian, G.-D.; Chen, B. Emerging Multifunctional Metal-Organic Framework Materials. *Adv. Mater.* **2016**, *28*, 8819−8860.

(7) Li, Y.-A.; Zhao, C.-W.; Zhu, N.-X.; Liu, Q.-K.; Chen, G.-J.; Liu, J.-B.; Zhao, X.-D.; Ma, J.-P.; Zhang, S.; Dong, Y.-B. Nanoscale UiO-MOFs-based Luminescent Sensors for Highly Selective Detection of Cysteine and Glutathione and Their Application in Bioimaging. *Chem. Commun.* **2015**, *51*, 17672−17675.

(8) (a) Schaate, A.; Roy, P.; Godt, A.; Lippke, J.; Waltz, F.; Wiebacke, M.; Behrens, P. Modulated Synthesis of Zr-Based Metal−Organic Frameworks: From Nano to Single Crystals. *Chem. - Eur. J.* **2011**, *17*, 6643−6651. (b) Horcajada, P.; Chalati, T.; Serre, C.; Gillet, B.; Sebrie, C.; Baati, T.; Eubank, J. F.; Heurtaux, D.; Clayette, P.; Kreuz, C.; Chang, J.-S.; Hwang, Y. K.; Marsaud, V.; Bories, P.-N.; Cynober, L.; Gil, S.; Férey, G.; Couvreur, P.; Gref, R. Porous Metal−Organic-Framework Nanoscale Carriers as a Potential Platform for Drug Delivery and Imaging. *Nat. Mater.* **2010**, *9*, 172−178.

(9) (a) Ruyra, À.; Yazdi, A.; Espin, J.; Carné-Sánchez, A.; Roher, N.; Lorenzo, J.; Imaz, I.; Maspoch, D. Synthesis, Culture Medium Stability, and In Vitro and In Vivo Zebrafish Embryo Toxicity of Metal−Organic Framework Nanoparticles. *Chem. - Eur. J.* **2015**, *21*, 2508−2518. (b) Park, J.; Jiang, Q.; Feng, D.; Mao, L.; Zhou, H.-C. Size-Controlled Synthesis of Porphyrinic Metal−Organic Framework and Functionalization for Targeted Photodynamic Therapy. *J. Am. Chem. Soc.* **2016**, *138*, 3518−3525. (c) Li, Y.-A.; Zhao, X.-D.; Yin, H.-P.; Chen, G.-J.; Yang, S.; Dong, Y.-B. Drug-Loaded Nanoscale Metal-Organic Framework with Tumor Targeting Agent for Highly Effective Hepatoma Therapy. *Chem. Commun.* **2016**, *52*, 14113−14116.

(10) Mei, J.; Hong, Y.; Lam, J. W. Y.; Qin, A.; Tang, Y.; Tang, B. Z. Aggregation-Induced Emission: The Whole Is More Brilliant than the Parts. *Adv. Mater.* **2014**, *26*, 5429−5479.

(11) (a) *CrysAlisPro, Version 1.171.36.32* (release 02-08-2013 CrysAlis 171. NET); Agilent Technologies (compiled Aug 2, 2013, 16:46:58). (b) Spek, A. L. *PLATON, A Multipurpose Crystallographic Tool*; University of Utrecht, Utrecht, The Netherlands, 1998.

(12) Gui, B.; Meng, X.; Chen, Y.; Tian, J.; Liu, G.; Shen, C.; Zeller, M.; Yuan, D.; Wang, C. Reversible Tuning Hydroquinone/Quinone Reaction in Metal−Organic Framework: Immobilized Molecular Switches in Solid State. *Chem. Mater.* **2015**, *27*, 6426−6431.

DOI: 10.1021/acs.inorgchem.7b02012
Inorg. Chem. XXXX, XXX, XXX−XXX